

## Supporting information

Belonging to the manuscript

### Crystal structure and *in situ* decomposition of $\text{Eu}(\text{BH}_4)_2$ and $\text{Sm}(\text{BH}_4)_2$

Terry D. Humphries,<sup>a,b</sup> Morten B. Ley,<sup>c</sup> Christoph Frommen,<sup>a</sup> Keelie T. Munroe,<sup>c</sup> Torben R. Jensen<sup>c</sup> and Bjørn C. Hauback<sup>a\*</sup>

<sup>a</sup> Physics Department, Institute for Energy Technology, P.O. Box 40, NO-2027, Kjeller, Norway. Fax: +47 63 81 09 20; Tel: +47 97 40 88 44.

<sup>b</sup> WPI-Advanced Institute for Materials Research, Tohoku University, 2-1-1 Katahira, Aoba-ku, Sendai 980-8577, Japan.

<sup>c</sup> Centre for Materials Crystallography (CMC), Interdisciplinary Nanoscience Center (iNANO) and Department of Chemistry, University of Aarhus, Langelandsgade 140, DK-8000 Århus C, Denmark. Fax: +45 8619 6199; Tel.: +45 8942 3894.

E-mail: [bjorn.hauback@ife.no](mailto:bjorn.hauback@ife.no)

#### Contents:

##### Synthesis of S1-4.

##### Thermal Decomposition of $\text{EuCl}_3 + 6\text{LiBH}_4$ - S2.

**Fig. E1:** *In situ* SR-PXD data of S2.

**Fig. E2:** Thermal analysis of S2 by TGA-MS.

##### Thermal Decomposition of $\text{EuCl}_2 + 2\text{LiBH}_4$ - S3.

**Fig. E3:** *In situ* SR-PXD data of milled  $\text{EuCl}_2$  and  $2\text{LiBH}_4$  (S3).

**Fig. E4:** Desorption of S3 by Sieverts measurements over three hydrogenation cycles.

**Fig. E5:** *Ex situ* powder X-ray diffractogram of S3 after ball milling (1) and annealing (2).

**Fig. E6:** Thermal analysis of S4.

**Fig. E7:** ATR FT-IR spectra of the prepared samples S1-S4.

**Table E7:** FT-IR Vibrations of Measured for S1-S4 compared to other borohydride complexes ( $\text{cm}^{-1}$ ).

## Synthesis of S1 - S4

**Solution Synthesis of  $\text{Eu}(\text{BH}_4)_2$  (S1)** A 3:1 ratio of  $\text{LiBH}_4$  and  $\text{EuCl}_3$  were weighed into a glass vessel, to which 30 mL  $\text{Et}_2\text{O}$  was added by syringe and the mixture allowed to stir overnight. The  $\text{Et}_2\text{O}$  was removed *in vacuo* resulting in a grey powder before 30 mL of  $\text{Me}_2\text{S}$  being added to the vessel and the suspension stirred overnight. The resultant mixture was filtered using standard solvent-based extraction techniques.<sup>1</sup> The remaining  $\text{Me}_2\text{S}$  was removed *in vacuo* leaving a yellow/green powder behind.

**Mechano-chemical synthesis and solvent extraction of  $\text{Eu}(\text{BH}_4)_2$  (S2)**  $\text{LiBH}_4$  and  $\text{EuCl}_3$  were weighed in a 6:1 ratio into a stainless steel BM vial with stainless steel balls, employing a ball to powder ratio of 40:1. The sample was ball-milled using a Fritsch Pulverisette 7 planetary mill under inert conditions (argon atmosphere) for 5 h at 400 rpm. An aliquot of the powder was weighed into a glass vessel, to which 30 mL  $\text{Me}_2\text{S}$  was added by syringe and the mixture allowed to stir overnight. The resultant mixture was filtered using standard solvent-based extraction techniques.<sup>1</sup> No powder was evident in the filtrate after removal of  $\text{Me}_2\text{S}$ . The residue was subsequently used for analysis.

**Mechano-chemical synthesis of  $\text{Eu}(\text{BH}_4)_2$  (S3)**  $\text{LiBH}_4$  and  $\text{EuCl}_2$  were weighed in a 2:1 ratio into a tungsten carbide BM vial with tungsten carbide balls, employing a ball to powder ratio of 30:1. The sample was ball-milled using a Fritsch Pulverisette 6 planetary mill under inert conditions (argon atmosphere) in repeated sequences for 48 repetitions applying 5 min BM and 2 min pauses with a speed of 450 rpm. The resultant sample was light yellow. The sample was annealed at 250 °C for 45 min at 100 bar  $\text{H}_2$  to ensure complete reaction between  $\text{EuCl}_2$  and  $\text{LiBH}_4$ .

**Solution Synthesis of  $\text{Sm}(\text{BH}_4)_2$  (S4)**  $\text{LiBH}_4$  and  $\text{SmCl}_3$  were added in a 3:1 ratio to a glass vessel. 30 ml  $\text{Et}_2\text{O}$  was added and the mixture was allowed to stir overnight.  $\text{Et}_2\text{O}$  was removed *in vacuo* resulting in a grey mixture.  $\text{Me}_2\text{S}$  was added and allowed to stir overnight. The resultant mixture was filtered using standard solvent-based extraction techniques.<sup>1</sup> The remaining  $\text{Me}_2\text{S}$  was removed *in vacuo* leaving a very sticky light brown solid. The sample was then heated for 2 h at 140 °C under dynamic vacuum yielding a dark purple solid.

## Thermal Decomposition of $\text{EuCl}_3 + 6\text{LiBH}_4$ - S2

A sample of  $\text{EuCl}_3$  was reacted with  $6\text{LiBH}_4$  by mechano-milling in a stainless steel vial under inert atmospheric conditions (S2). The X-ray amorphous product was consequently stirred in  $\text{Me}_2\text{S}$  yielding a crystalline product upon removal of solvent. S2 was analysed by *in situ* SR-PXD, DSC, TGA and MS and the results illustrated in Figs. E1 and E2. Analysis of the initial diffraction pattern, measured at RT, portrays that the powder contains  $\text{LiCl}$  and  $\text{EuCl}_2$ .<sup>2</sup> Another crystalline compound is also apparent, possibly a  $\text{Eu}(\text{BH}_4)_2$  solvated phase in accord, while the mass loss of 3.4 wt% measured by TGA and  $\text{Me}_2\text{S}$  detected by MS in the temperature range of 70 and 108 °C can be attributed to the sample being insufficiently dried prior to the experiment (Fig. E2). This event culminates in the first observable crystallographic phase transformation. Phase analysis of the

sample at  $\sim 135$  °C by Rietveld refinement indicates a composition of  $\text{Eu}(\text{BH}_4)_2$  36.019(10) wt%,  $\text{EuCl}_2$  17.52(2) wt%, and  $\text{LiCl}$  46.46(2) wt%.

At ca. 165 °C, the  $\text{Eu}(\text{BH}_4)_2$  phase becomes amorphous giving way to a mixture containing  $\text{EuCl}_2$  and  $\text{LiCl}$  as the major crystalline phase, along with a minor phase which continues to increase in concentration throughout the course of the experiment. A mass loss of 11.5 wt% is measured between 108 and 224 °C complemented with the detection of some  $\text{Me}_2\text{S}$  and  $\text{B}_2\text{H}_6$ . This phenomenon was also observed in the previous sample (S1) and is attributed to solvent desorption from the  $\text{Eu}(\text{BH}_4)_2 \cdot x\text{Me}_2\text{S}$  adduct. This emission is followed by the formation of a new compound which is present between 224 and 347 °C. Unfortunately, the material was unable to be indexed and did not match any known material in the ICSD database. During the temperature range of 224 and 259 °C, a further mass loss of 1.3 wt% is observed along with a small quantity of  $\text{H}_2$ . This can be attributed to the first  $\text{H}_2$  release from  $\text{Eu}(\text{BH}_4)_2$ .

Between 334 and 389 °C the main desorption of  $\text{H}_2$  occurs, with an accompanied weight loss of 1.56 wt%, which could be the second  $\text{H}_2$  release from  $\text{Eu}(\text{BH}_4)_2$ . A final reaction is observed at  $\sim 384$  °C including oxidation products, e.g. europium borates such as  $\text{EuBO}_3$ .

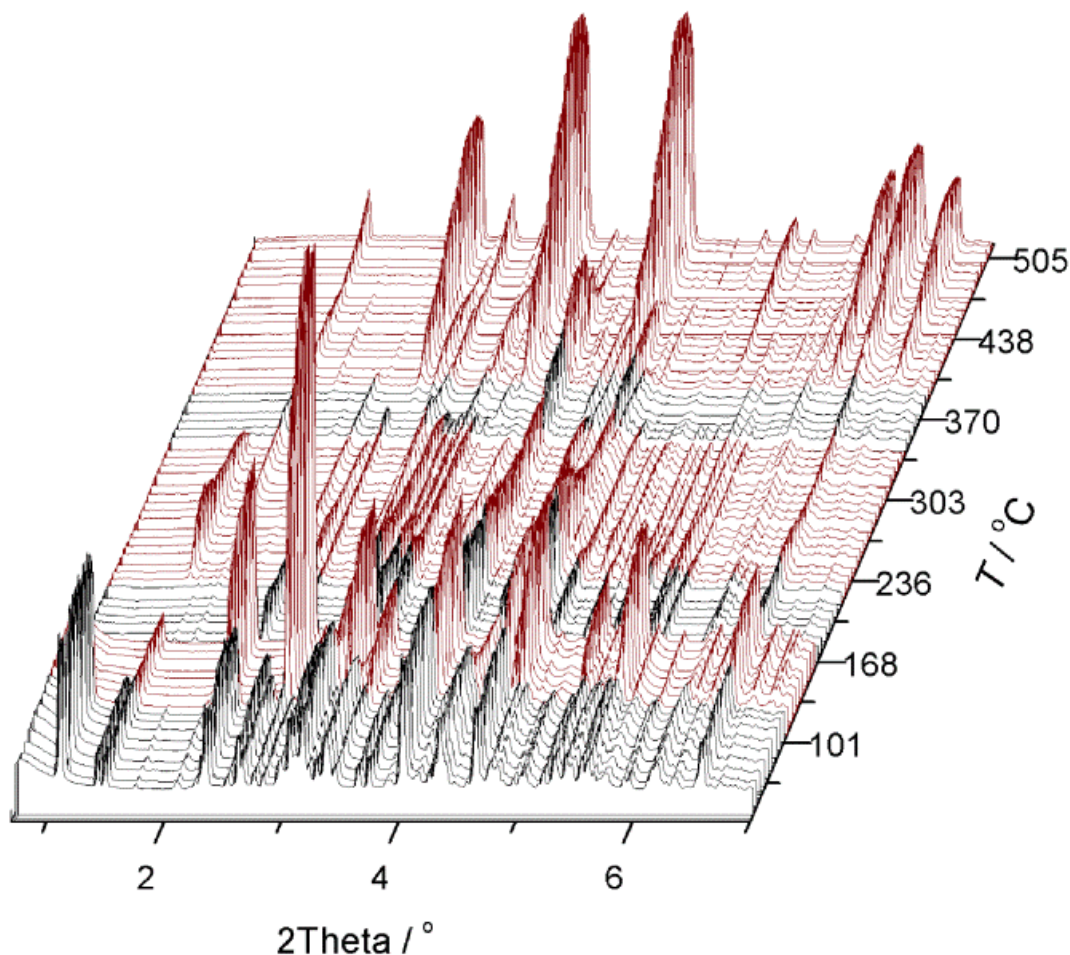


**Fig. E1.** *In situ* SR-PXD data of S2 ( $\Delta T/\Delta t = 5$  °C/min,  $\lambda = 0.2072$  Å).

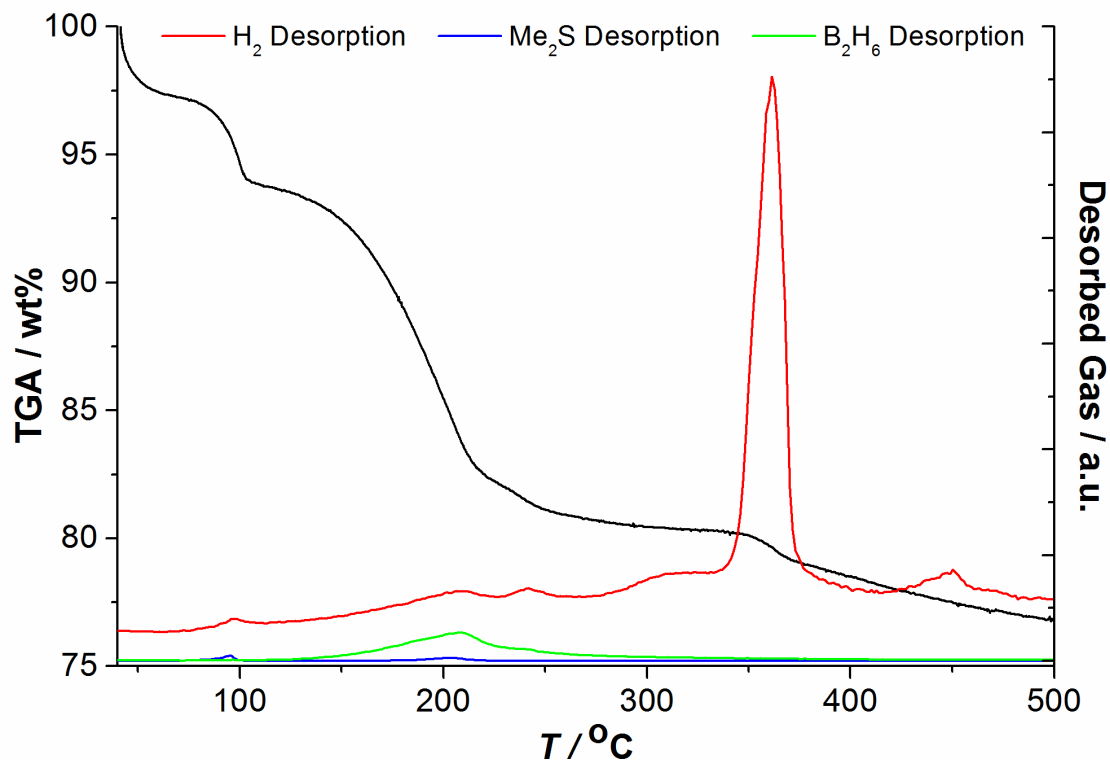


**Fig. E2.** Thermal analysis of S2 by TGA-MS ( $\Delta T/\Delta t = 5 \text{ }^\circ\text{C}/\text{min}$ ).

### Thermal Decomposition of $\text{EuCl}_2 + 2\text{LiBH}_4 - \text{S3}$

A sample of  $\text{EuCl}_2$  was reacted with two equivalents of  $\text{LiBH}_4$  by BM (S3) and the powder analysed by *in situ* SR-PXD and PCT measurements (Figs. E3 and E4). Analysis of the initial diffraction pattern, measured at RT, portrays that the powder contains  $\text{LiCl}$  and  $\text{EuCl}_2$ , and another unidentified crystalline compound. The decomposition of this material is complicated and analysis of the PXD data is marred by the presence of the starting materials. However, the formation of  $\text{Eu}(\text{BH}_4)_2$  is observed during heating of the sample starting at  $120 \text{ }^\circ\text{C}$  and at  $250 \text{ }^\circ\text{C}$   $\text{Eu}(\text{BH}_4)_2$  is the major crystalline phase, before disappearing at  $\sim 295 \text{ }^\circ\text{C}$ .

In order to encourage the complete reaction of the milled starting materials, the powder was annealed at  $250 \text{ }^\circ\text{C}$  for 45 min, under 100 bar  $\text{H}_2$ . After *ex situ* PXD analysis of the resultant powder (Fig. E5), only  $\text{Eu}(\text{BH}_4)_2$  and  $\text{LiCl}$  are observed, determining that the reaction may be thermodynamically hindered. Annealing of the sample may also aid the reaction to overcome some kinetic limitations, with the temperature being required to drive the reaction to completion. In contrast, the reactions carried out in solvent conditions are successfully driven to completion by solvent interaction and stabilisation.

The decomposition of S3 after annealing, observed by PCT measurements (Fig. E4), indicates a two-step desorption process. The first inflection occurs at  $\sim 250 \text{ }^\circ\text{C}$  and concludes after  $\sim 350 \text{ }^\circ\text{C}$ . The second process ensues immediately, at a much faster rate than the first, concluding at  $>420 \text{ }^\circ\text{C}$ .

A total of 2.5 wt% H<sub>2</sub> is desorbed up to 450 °C, lower than the theoretical 4.4 wt%, possibly due to the LiCl impurity in the sample.

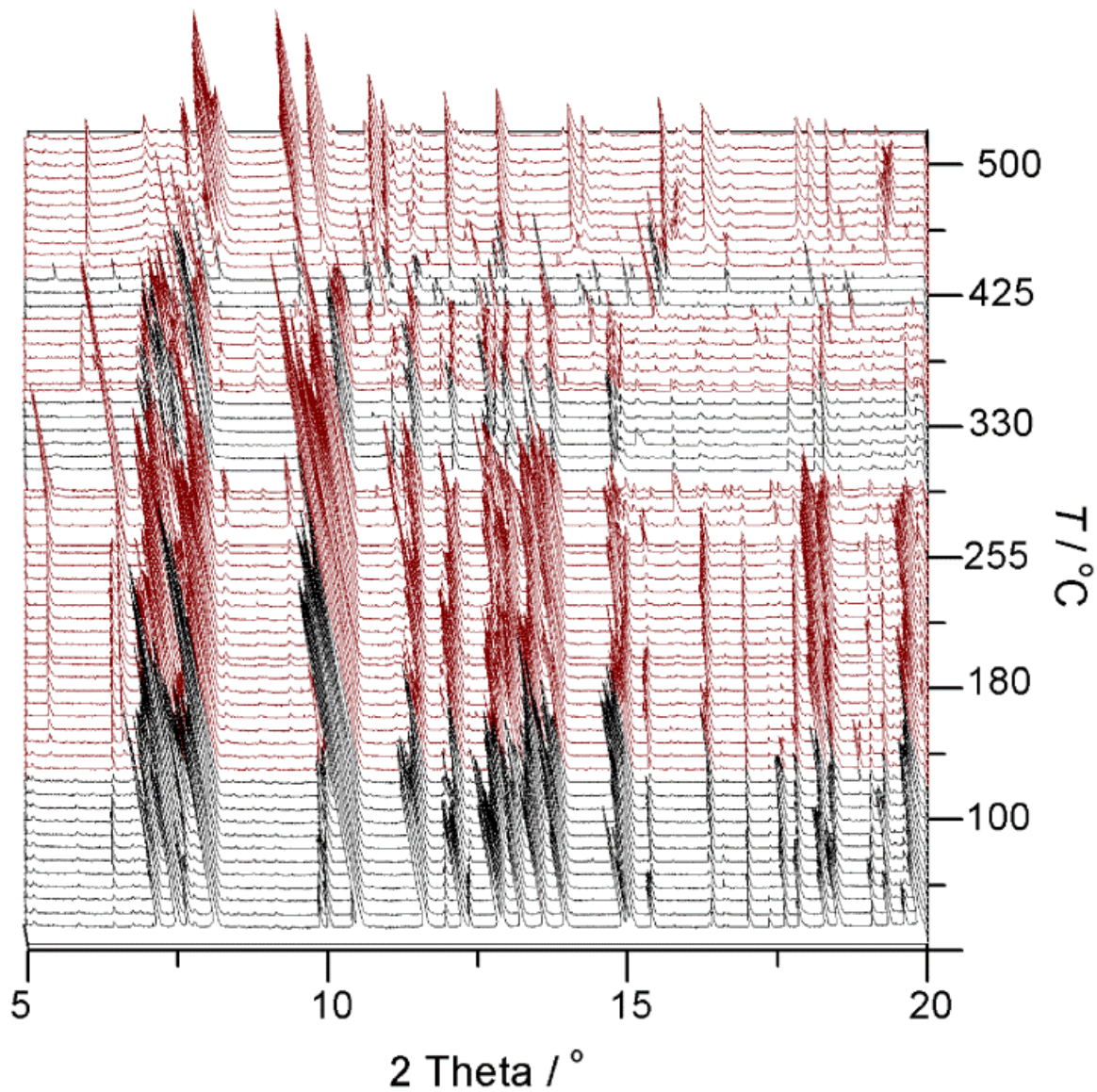


**Fig. E3.** *In situ* SR-PXD data of milled EuCl<sub>2</sub> and 2LiBH<sub>4</sub> (S3) ( $\Delta T/\Delta t = 5^\circ\text{C}/\text{min}$ ,  $\lambda = 0.5053 \text{ \AA}$ ).

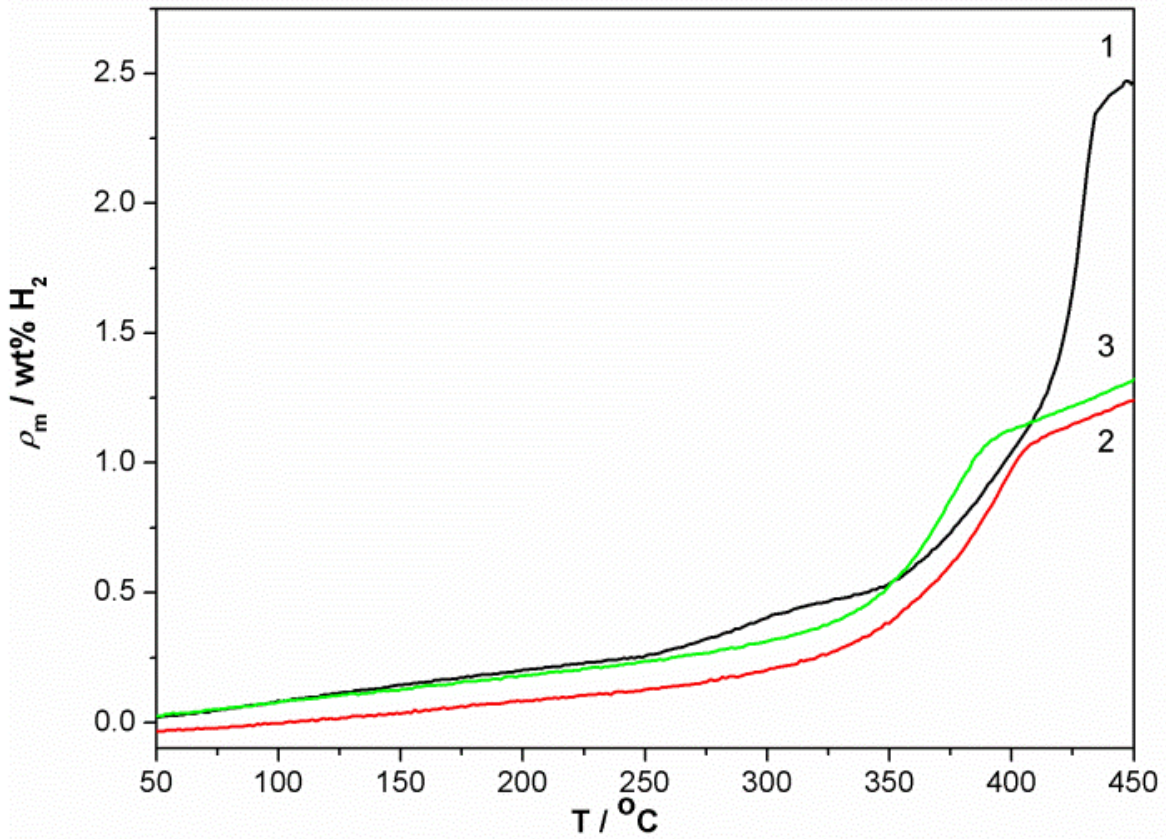


**Fig. E4.** Desorption of S3 by Sieverts measurements over three hydrogenation cycles ( $\Delta T/\Delta t = 3$  °C/min,  $p(\text{H}_2) = 1$  bar). Hydrogen absorption measurements were performed at 400 °C and  $p(\text{H}_2) = 100$  bar for 8 h.

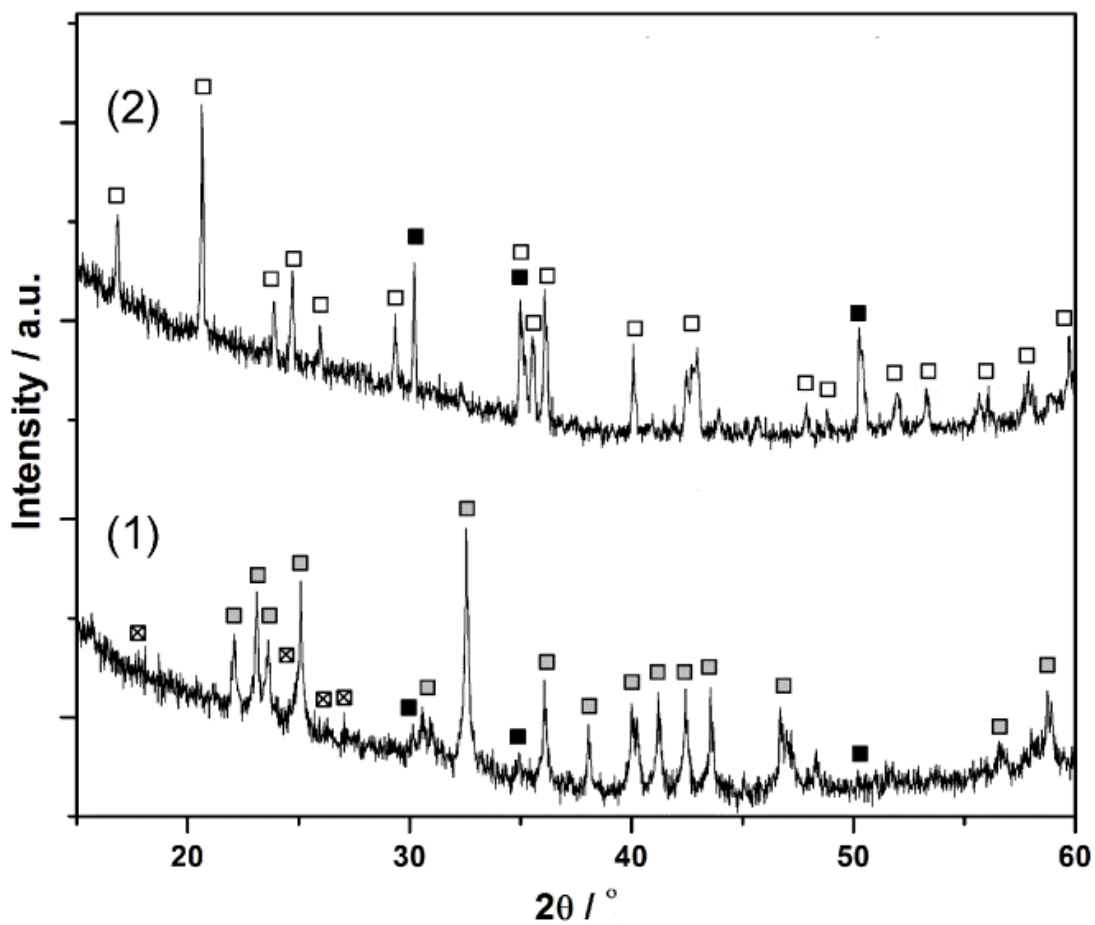


**Fig. E5.** *Ex situ* powder X-ray diffractogram of S3 after ball milling (1) and annealing (2) ( $\lambda = 1.5406 \text{ \AA}$ ). Symbols: grey square  $\text{EuCl}_2$ , cross square  $\text{LiBH}_4$ , white square  $\text{Eu}(\text{BH}_4)_2$ , black square  $\text{LiCl}$ .

---

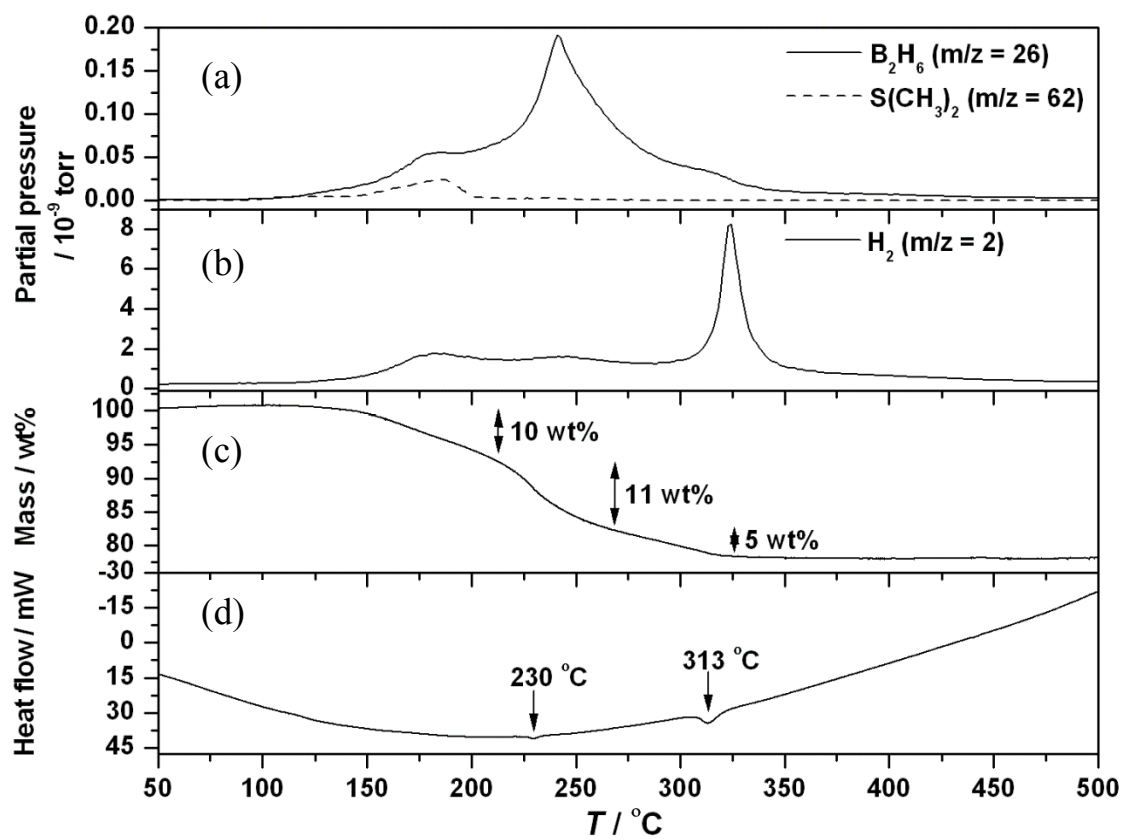


**Fig. E6** Thermal analysis of S4. MS ((a)  $\text{Me}_2\text{S}$  and  $\text{B}_2\text{H}_6$  (b)  $\text{H}_2$ ), (c) TGA and (d) DSC were measured simultaneously ( $\Delta T/\Delta t = 5^\circ\text{C}/\text{min}$ ).

## FT-IR Spectroscopy

The ATR FT-IR spectra of S1-S4 illustrated in Fig. E6 and Table E1 details some important similarities and differences between the prepared samples. The most important similarity is the strong broad band in the region of  $2290\text{ cm}^{-1}$  attributed to B–H stretching modes. This band is common for all borohydrides, for example  $\text{Mn}(\text{BH}_4)_2$  ( $2223\text{ cm}^{-1}$ ),  $\text{LiBH}_4$  ( $2276$  and  $2303\text{ cm}^{-1}$ ) and  $\text{NaSc}(\text{BH}_4)_4$  ( $2240$  and  $2392\text{ cm}^{-1}$ ).<sup>3-5</sup> In the spectra of S1, S2 and S4, a vibration is observed at ca.  $1380\text{ cm}^{-1}$  which is attributed to B–H bridging bending mode. This mode is also very common in borohydride complexes and shown in detail in the vibrational spectroscopy study of  $\text{Mn}(\text{BH}_4)_2$ .<sup>4</sup> The terminal B–H stretching modes, normally observable in the  $2400 - 2500\text{ cm}^{-1}$  region, may be obscured by the very broad B–H stretching mode but seen as a shoulder in the S3 spectrum at  $2393\text{ cm}^{-1}$  and more prominently in S4 at  $2426\text{ cm}^{-1}$ . Desorption of  $\text{Me}_2\text{S}$  solvent observed in the thermal analysis is corroborated by the IR spectra of S1, S2 and S4, where a multiplet in the  $2900\text{ cm}^{-1}$  region, corresponding to aliphatic C–H stretching is observable. The peak at  $1630\text{ cm}^{-1}$  is attributed to a  $\text{H}_2\text{O}$  bending mode as the samples were measured in air, albeit exposed for as short as possible. O–H stretching modes are also observed at  $3500\text{ cm}^{-1}$ .

The fingerprint region of the spectra for S1, S2 and S4 are not as pronounced as that of S3, which is likely due to sample thickness and preparation, as well as solvent interactions. Only one deformation vibration is common for each sample measured in this study, which occurs at  $\sim 1080\text{ cm}^{-1}$ .

The relative simplicity of the spectra for samples S1-4 corroborates the crystal structure of the divalent *RE* borohydrides. A large variety of covalent bonds within a structure would entail a complicated spectra, as shown in the afore section, the covalent bonds in  $\text{Eu}$  and  $\text{Sm}(\text{BH}_4)_2$  are limited to B–H bonds. Bridging bending modes are observed in samples S1-S4 denoting that there are two types of B–H bond in the structure. Unfortunately, terminal stretching modes are not observed for S1 and S2 as they are likely engulfed by the broad B–H stretching modes at ca.  $2280\text{ cm}^{-1}$ .

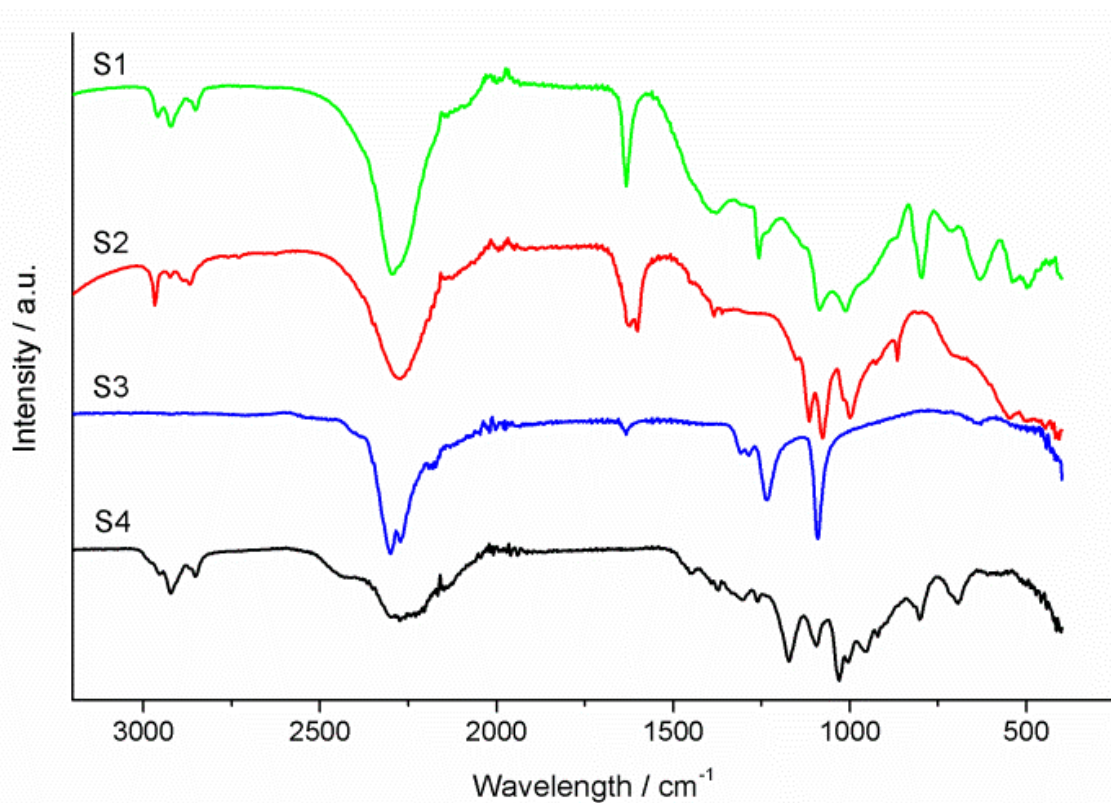


**Fig. E7.** ATR FT-IR spectra of the prepared samples S1-S4.

**Table E1.** IR Vibrations measured for S1-S4 compared to other borohydride complexes ( $\text{cm}^{-1}$ ).

Compound	Deformation modes	Bridging bending mode	B–H stretching modes + Fermi resonances	Terminal B–H stretching modes
S1	1077 s	1361 w	2272 sbr	---
S2	1086 s	1378 w	2295 sbr	---
S3	1091 s	1309 w	2272, 2300 sbr	2395 sh
S4	1176 s, 1100 s, 1031 s	1307 w	2150 sh, 2268 br	2426 mbr
$\text{Mn}(\text{BH}_4)_2^a$	1093 sh, 1106, 1205	1349	2223 br	---
$\text{NaSc}(\text{BH}_4)_4^b$	1105, 1187	1340 w	2240, 2392	2459, 2486

s strong; m medium; w weak; br broad; sh shoulder; <sup>a</sup>Ref 4; <sup>b</sup>Ref 3.

## References

1. H. Hagemann and R. Cerny, *Dalton Trans.*, 2010, 39, 6006-6012.
2. S. Marks, J. G. Heck, M. H. Habicht, P. Ona-Burgos, C. Feldmann and P. W. Roesky, *J. Am. Chem. Soc.*, 2012, 134, 16983-16986.
3. R. Cerny, G. Severa, D. B. Ravnsbæk, Y. Filinchuk, V. D'Anna, H. Hagemann, D. Haase, C. M. Jensen and T. R. Jensen, *J. Phys. Chem. C*, 2010, 114, 1357-1364.
4. G. Severa, H. Hagemann, M. Longhini, J. W. Kaminski, T. A. Wesolowski and C. M. Jensen, *J. Phys. Chem. C*, 2010, 114, 15516-15521.
5. V. D'Anna, A. Spyratou, M. Sharma and H. Hagemann, *Spectrochim. Acta Mol. Biomol. Spectros.*, 128, 902-906.